coatings

MDPI

Article

The Influence of CO_2-Cured Boiler Cinder on the Mechanical Strength of RPC Exposed to NaCl Erosion

Ligai Bai [1], Haiyuan Liu [2] and Hui Wang [3,*]

[1] School of Architectural Engineering, North China Institute of Aerospace Engineering, Langfang 065000, China; bailigai@aliyun.com
[2] China Construction First Group Co., Ltd., 52 South West Sihuan Road, Beijing 100161, China; liuhaiyuan@aliyun.com
[3] School of Civil Engineering and Geographic Environment, Ningbo University, Ningbo 315000, China
* Correspondence: huiwang123@aliyun.com

Abstract: Boiler cinder is a kind of mining waste that may cause environmental pollution. Based on this reason, a processing method needs to be carried out. In this study, the influence of CO_2-cured boiler cinder on the compressive and flexural strengths of reactive powder cement concrete (RPC) under NaCl actions is investigated. The mass loss rates (MLR) and the relative dynamic modulus of elasticity (RDME) are measured to reflect the resistance of NaCl erosion. The thermogravimetric analysis (TGA), scanning electron microscope (SEM), and X-ray diffraction (XRD) spectrum are obtained for revealing the mechanism of the macro performance. Results show that the relationship between the MLR and the mass ratio of CO_2-cured boiler cinder fits the quadratic function with NaCl erosion. Meanwhile, the MLR during NaCl action are decreased by increasing the amount of CO_2-cured boiler cinder. The MLR range from 0% to 5.3% during NaCl action, and the decreasing rate of MLR by CO_2 curing on boiler cinder is 0%–51.3%. The function of RDME and the mass ratio of CO_2-cured boiler cinder accords with the positive correlation quadratic function. The mechanical strengths decrease when NaCl erosion is encountered. The mechanical strengths' decreasing rates of RPC are elevated with the increasing number of NaCl freeze–thaw cycles and the NaCl dry–wet alternations. The increasing rates of flexural and compressive strengths of RPC by 13.1%–36.3% and 11.2%–50.4% are achieved by adding CO_2-cured boiler cinder. As observed from the TGA and SEM's results, the addition of CO_2-cured boiler cinder can increase the thermogravimetric value and the compactness of hydration products.

Keywords: boiler cinder; CO_2-cured; reactive powder cement concrete; thermogravimetric analysis; X-ray diffraction spectrum

Citation: Bai, L.; Liu, H.; Wang, H. The Influence of CO_2-Cured Boiler Cinder on the Mechanical Strength of RPC Exposed to NaCl Erosion. *Coatings* **2023**, *13*, 1021. https://doi.org/10.3390/coatings13061021

Academic Editor: Andrea Nobili

Received: 16 May 2023
Revised: 25 May 2023
Accepted: 29 May 2023
Published: 31 May 2023

1. Introduction

Boiler cinder is a solid waste produced by coal combustion. Billions of tons of furnace ash is produced every year. If boiler cinder has not been disposed of timely, it causes serious pollution in the environment [1]. The accumulation of boiler cinder can pollute air and water sources. Currently, stacking and landfill methods are commonly used to treat furnace ash. However, this method has caused a significant waste of resources. Therefore, some significant methods should be taken to address the issue of boiler ash treatment.

Boiler cinder can be applied in manufacturing masonry mortar and wall materials [2]. Moreover, some boiler cinder has been used as lightweight concrete aggregate [3]. Some researchers point out that boiler cinder can be used for making lightweight concrete aggregates with a density of 1800 kg/m^3 [4]. Moreover, some scholars point out that boiler cinder can be used as aggregates in asphalt concrete [5]. Liu reported that boiler cinder can be used as roof insulation or indoor foundation material, while coal slag can also be used as road building materials, sandblasting sand, etc. [6]. Above all, boiler cinder has been utilized as cementitious material due to the hydration activity [7].

Cement concrete is still one of the most widely used materials to date [8]. The production of cement consumes a large amount of resources and energy [9]. Based on these reasons, active substances (mineral admixtures, waste fly ash, and furnace ash) are used to replace cement [10]. As obtained from Cui's research, the flexural and compressive strengths of reactive powder cement concrete can be increased by 32.4% and 23.7%, respectively, by adding waste fly ash (0%–25%) [11]. Moreover, the reinforced RPC's corrosion resistance can be improved with waste fly ash [12]. However, as found in Du's research [13], RPC with waste fly ash can leach out some toxic heavy metals, which will pollute the environment. Therefore, it is necessary to provide harmless materials.

RPC is a type of ultra-high-performance concrete invented in the 1990s, which exhibits a compressive strength higher than 100 MPa and extremely high durability [14,15]. Boiler cinder is a solid waste produced without any pollution. Boiler cinder performs a certain content of cement hydration-active substances, which may be effective for the mechanical strengths and the long-term performance of RPC [16]. However, few journals about this are reported.

CO_2 is the gas that will accelerate the greenhouse effect with excessive emission [17]. Treating solid waste with CO_2 can consume excessive CO_2 gas, thus improving the corresponding performance [18–21]. CO_2-cured bird nest may provide further improvement for the performance of RPC. So far, few studies on this aspect of research have been reported.

In this study, the influence of CO_2-cured boiler cinder on the mechanical strengths of RPC is studied. The influence of NaCl freeze–thaw cycles (F-C) and dry–wet alternations (D-A) is considered. The mass loss rates (MLR) and the relative dynamic modulus of elasticity (RDME) are determined for the characterization of NaCl erosion on reactive powder cement concrete. The mechanism of the macro performance is revealed by the thermogravimetric analysis (TGA), X-ray diffraction (XRD) spectrum, and scanning electron microscope (SEM).

2. Experimental

2.1. Raw Materials

The ordinary Portland cement (OPC) used in this research is provided by Langfang Hongke Cement Products Co., Ltd., Langfang, China. The cement shows an initial setting time of 103.5 min and a final setting time of 313.2 min. The compressive strength grade of this cement is 42.5 MPa. Silica fume (SF) with a density of 281.3 kg/m^3, SiO_2 content of 95%, and melting point of 1600 °C is used as a kind of mineral admixture in this study. The boiler cinder (BC) is provided by Shanghai Qinwang Environmental Protection Materials Co., Ltd., Shanghai, China. Tables 1 and 2 show the particle size and compositions of the binder materials. The quartz sand is used as fine aggregate of RPC, which is provided by Lingshou County Zechuang Mineral Products Co., Ltd., Lingshou, China. The size ranges of the quartz sand are 0.67–1.22 mm, 0.31–0.63 mm, and 0.13–0.35 mm. The mass ratios of these quartz sand are 1:1.5:1. A polycarboxylate superplasticizer with a water reducing rate of 37.8% is applied for adjusting the fluidity of fresh RPC.

Table 1. The accumulated pass rate of the binder materials (%).

Types	Particle Size/μm						
	0.3	**0.6**	**1**	**4**	**8**	**64**	**360**
OPC	0.11	0.32	2.4	15.3	28.3	93.4	100
GGBS	0.042	0.13	3.28	19.38	35.17	98.18	100
SF	31.28	58.49	82.38	100	100	100	100
Quartz sand	0	0	0	0	0.039	23	100
BC	0.15	0.41	0.82	1.13	5.96	20.4	100

Table 2. Chemical composition of the cementitious materials (%).

Types	SiO_2	Al_2O_3	Fe_xO_y	MgO	CaO	SO_3	K_2O	Na_2O	Ti_2O	Loss on Ignition
OPC	20.8	5.6	3.8	1.8	62.1	2.8	-	-	-	3.1
GGBS	34	14.9	0.5	9.8	36.9	0.3	3.6	-	-	-
SF	90.8	0.21	0.62	0.23	0.44	0.2	7.5	-	-	-
Quartz sand	99.8	-	0.2	-	-	-	-	-	-	-
BC	52.10	18.34	11.99	4.85	6.61	-	1.57	2.43	0.87	-

2.2. The Manufacturing Process of Specimens

All binder materials and the quartz sand are added and mixed in a UJZ-15 mixer and stirred for 2 min. After that, the mixed solution with water and a water-reducing agent is added to the materials. Another 3 min is provided for mixing the materials. When the mixing is finished, fresh RPC is poured to the molds with sizes of 40 × 40 × 160 mm^3 and 100 × 100 × 400 mm^3. Specimens with a size of 40 × 40 × 160 mm^3 are used for flexural and compressive strengths. Meanwhile, specimens with a size of 100 × 100 × 400 mm^3 are applied for measuring the MLR and RDEM. The manufacturing process of RPC is shown in Figure 1. Table 3 shows the mixing proportions of RPC. In Table 3, silica fume (SF) is replaced gradually (0%, 25%, 50%, 75%, and 100%) by boiler cinder (BC) in individual compositions.

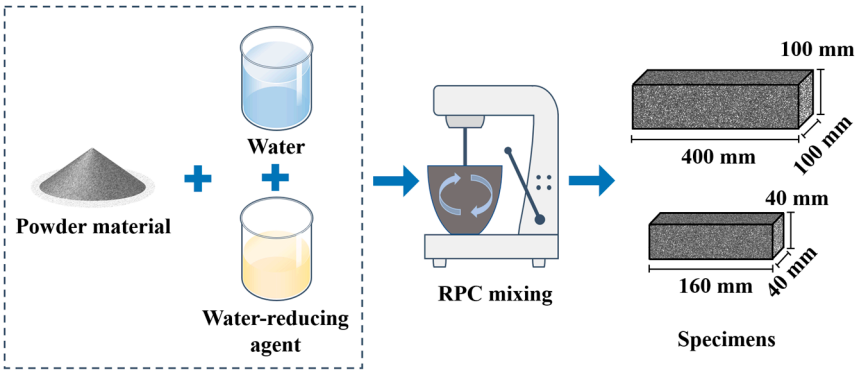

Figure 1. The manufacturing process of RPC specimens.

Table 3. The mixing proportions of RPC (kg/m^3).

Water	OPC	BC	SF	GGBS	Quartz Sand	Water Reducer
244.4	740.7	0	370.3	111.1	977.9	16.3
244.4	740.7	92.6	277.7	111.1	977.9	16.3
244.4	740.7	185.2	185.2	111.1	977.9	16.3
244.4	740.7	277.7	92.6	111.1	977.9	16.3
244.4	740.7	370.3	0	111.1	977.9	16.3

2.3. Measurement of Mechanical Strengths

The fully automatic bending and bending integrated testing machine is used for the measurement of flexural and compressive strengths. The loading speeds of the flexural experiment and the compressive experiment are 0.01 and 2.4 kN/s, respectively. Three specimens of each mixture are selected for the flexural strength. When each specimen is bent to two blocks, six blocks of every group are moved for the determination of the compressive strength. The average values of the mechanical strengths are considered as the experimental values of this research. Figure 2 shows the testing process of mechanical strengths. The mechanical strengths are carried out following the Chinese standard GB/T17671-1999 [22].

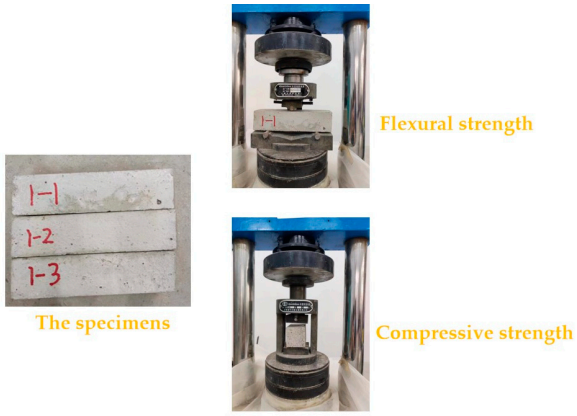

Figure 2. The equipment of mechanical strengths.

2.4. Experiments of NaCl F-C and D-A

The specimens standard-cured for 24 days are immersed in solution with a concentration of 3% for 4 days. When the immersion is finished, the specimens are moved to the TDR-1-type rapid freeze–thaw test box for concrete made by Hebei Tianjian Engineering Instrument Co., Ltd., Cangzhou, China, and the Tingyi Salt Dry Wet Cyclic Corrosion Test Chamber, Shanghai Tingyi Instrument Equipment Factory, Shanghai, China, for the measurement of NaCl F-C and NaCl D-A, respectively. The temperature of F-C is −15–8 °C. During the freeze–thaw experiment, the specimens are immersed in tubes filled with 3% NaCl. The experiment of NaCl D-A is described as follows.

All specimens are dried at a temperature of 80 °C for 15 h; after that, the dried specimens are cooled in the natural environment for 1 h. After cooling, all the specimens are immersed in NaCl solution for 8 h. After all these steps, a NaCl dry–wet alternation is finished. The MLR, the RDEM, and the loss rates of mechanical strengths are applied in reflecting the degree of performance degradation of NaCl F-C and D-A. The DT-W18A concrete dynamometer offered by Changzhou Dedu Precision Instrument Co., Ltd., Changzhou, China, is applied in the measurement of the relative dynamic modulus of elasticity. The measuring process is shown in Figure 3. The Chinese standard GB/T 50082-2009 [23] is used for the determination of NaCl F-C and D-A.

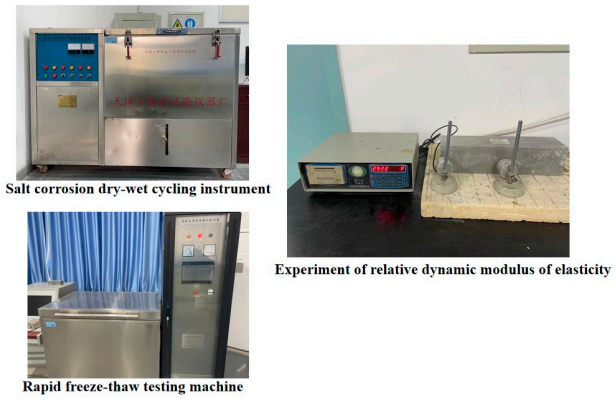

Figure 3. The equipment for NaCl F-C and D-A.

2.5. Microscopic Analysis Experiment

The powdered samples with a maximum particle size of 0.08 mm are applied to the determination of thermogravimetric analysis and the X-ray diffraction curves. A TGA-1150 thermogravimetric analyzer provided by Shanghai Junzhun Instrument Equipment Co., Ltd., Shanghai, China, is used for obtaining the TG curves. The temperature of the thermogravimetric analyzer ranges from 25 to 950 °C. A real-spectrum X-ray diffractometer offered by Suzhou Shipu Instrument Co., Ltd., Suzhou, China, is used for the XRD exper-

iment. Bean-shaped samples with a maximum particle size of 2.1 mm are used for the measurement of the SEM by a Zeiss scanning electron microscope (Guangdong Yuelian Instrument Co., Ltd., Guangzhou, China). The samples are dried in a vacuum drying oven at a temperature of 60 °C for 4 days. After drying, the samples are moved to a Zeiss scanning electron microscope for acquiring the SEM photos.

3. Results and Discussions

3.1. The MLR and RDEM of RPC during NaCl F-C

The MLR of RPC with CO_2-cured boiler cinder are shown in Figure 4. The MLR decrease in the form of quadratic function. The fitting degrees of all curves are higher than or equal to 0.98, indicating the accuracy of fitting results. This is attributed to the fact that the increasing dosages of CO_2-cured boiler cinder can reduce the pores in the boiler cinder [24]. Therefore, the freeze–thaw cracks are decreased by adding the CO_2-cured boiler cinder. The MLR are increased by the increasing number of F-C. This is mainly attributed to the fact that the inner cracks are accelerated and enlarged with the aggravated freeze–thaw effect [25]. Hence, some spalling on the surface of the specimens occurs, leading eventually to the increase in MLR. The maximum MLR of RPC during F-C ranges from 0% to 5.3%. The CO_2 curing on the boiler cinder can decrease the MLR by a maximum value of 51.3%.

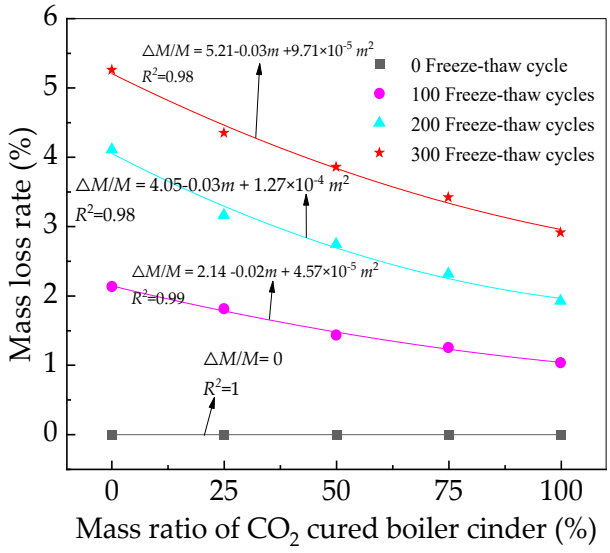

Figure 4. The MLR of RPC during NaCl F-C.

The relative dynamic modulus of elasticity of RPC with different dosages of CO_2-cured boiler cinder is shown in Figure 5. The RDME shows an increasing trend with the dosages of CO_2-cured boiler cinder due to the improved compactness of RPC by adding CO_2-cured boiler cinder [26]. Therefore, the increase in sound propagation speed leads to an increase in dynamic elastic modulus. However, the increased number of freeze–thaw cycles causes a decrease in RDME, which is attributed to the aggravated freeze–thaw damage by the increased number freeze–thaw cycles [27]. The relationship between the mass ratio of CO_2-cured boiler cinder and the RDME conforms to the relation of quadratic function. The fitting degrees are higher than or equal to 0.96, which shows the accuracy of the fitting equations. The RDME during F-C ranges from 100% to 83.2%. Meanwhile, CO_2 curing on boiler cinder can increase the RDME from 83.1% to 90.3%.

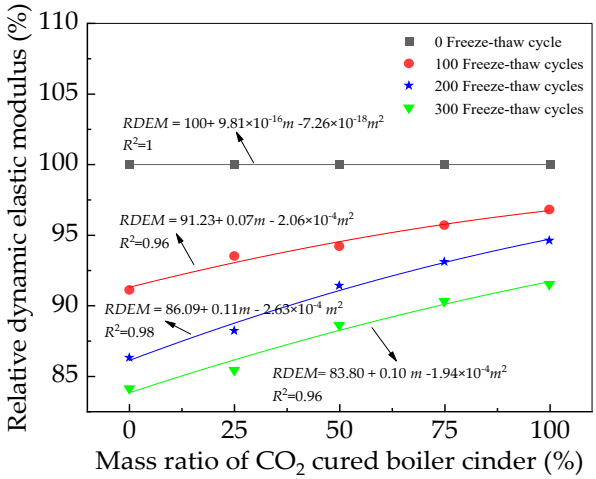

Figure 5. The RDEM of RPC during NaCl F-C.

3.2. The Mechanical Strengths of RPC NaCl F-C

The flexural and compressive strengths of RPC are exhibited in Figure 6. The mechanical strengths of RPC exhibit an increasing trend with the increasing dosages of CO_2-cured boiler cinder. However, when the number of F-C is increased, the mechanical strengths of RPC decrease. This is ascribed to the increased inner cracks by the freeze–thaw action [28]. The mechanical strengths' increasing rates of RPC with CO_2-cured boiler cinder increase with the increasing dosages of CO_2-cured boiler cinder due to the improved compactness of boiler cinder by the formed $CaCO_3$ of $Ca(OH)_2$ and CO_2 [29]. Moreover, the mechanical strengths' increasing rates by adding CO_2-cured boiler cinder are decreased with the increased number of NaCl freeze–thaw cycles. Comparing the flexural strength with the compressive strength, the increasing rate of the compressive strength is higher than that of the flexural strength's increasing rate. The increasing rates of the flexural and compressive strengths of RPC by 13.1%–36.3% and 11.2%–50.4% are achieved by adding CO_2-cured boiler cinder.

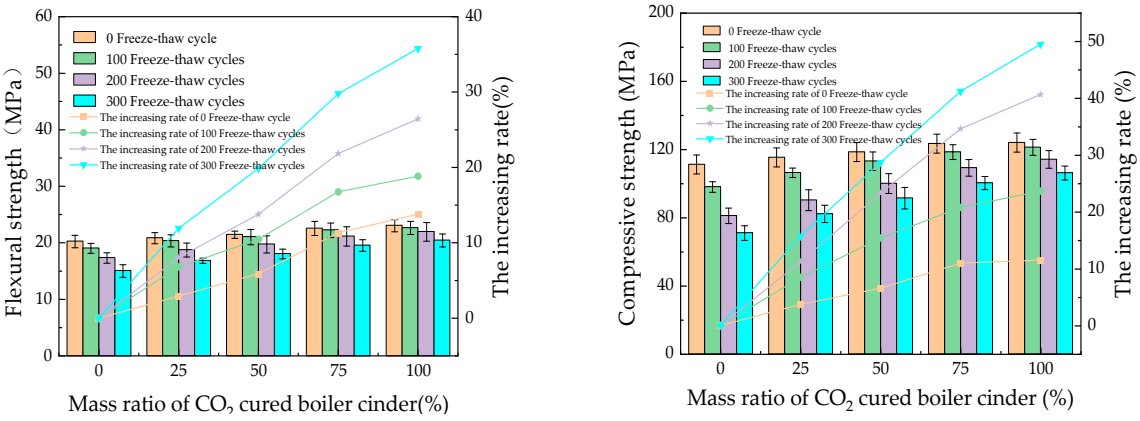

Figure 6. The mechanical strength of RPC during NaCl F-C. (**a**) The flexural strength; (**b**) the compressive strength.

3.3. The MLR and RDEM of RPC during NaCl D-A

The MLR of RPC during NaCl D-A are illustrated in Figure 7. The MLR decrease in the form of quadratic function with the mass ratio of CO_2-cured boiler cinder. The increased number of NaCl D-A has an increasing effect on the MLR. The MLR range from 0% to 5.78% during NaCl D-A. Meanwhile, the CO_2 curing can decrease the MLR from 5.78% to

3.72% after 30 NaCl D-A. This is attributed to the decreased internal defects in the sample and the increase in hydration products [30,31].

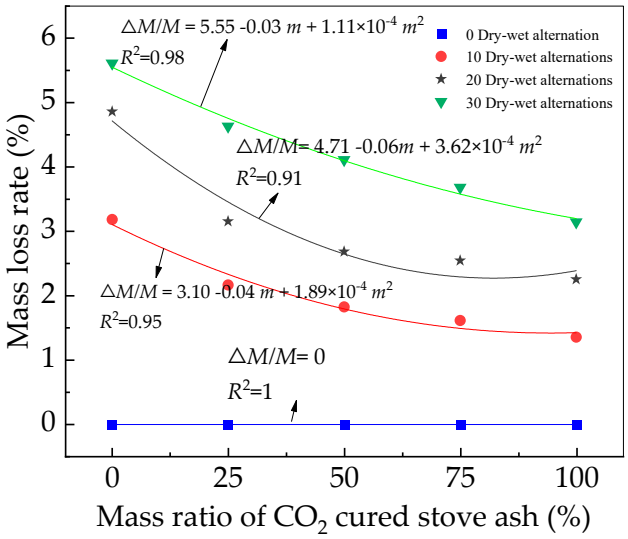

Figure 7. The MLR of RPC during NaCl D-A.

The RDEM of RPC with the increasing mass ratio of CO_2-cured boiler cinder is illustrated in Figure 8. As can be observed, the RDEM of RPC increases with the increasing content of CO_2-cured boiler cinder. Moreover, the increased number of NaCl D-A has an increasing effect on the RDEM of RPC. As can be found in Figure 8, the relationship between RDEM and m fits the quadratic function.

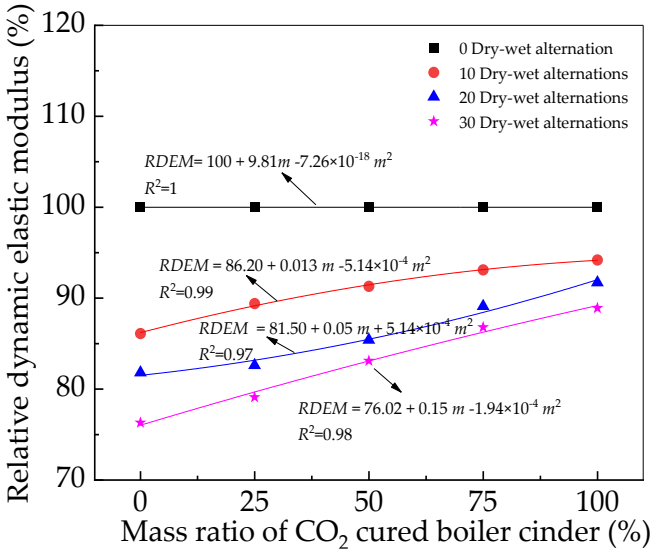

Figure 8. The RDEM of RPC during NaCl D-A.

The flexural and compressive strengths of RPC with CO_2-cured boiler cinder are illustrated in Figure 9a,b. As shown in Figure 9, the mechanical strengths increase with the addition of CO_2-cured boiler cinder and decreases with the NaCl dry–wet action. CO_2-cured boiler cinder can effectively improve the compactness of RPC, thus increasing the resistance to the NaCl dry–wet effect [32]. The NaCl dry–wet action increases internal damage of RPC with CO_2-cured boiler cinder, which leads to decreasing the mechanical strengths.

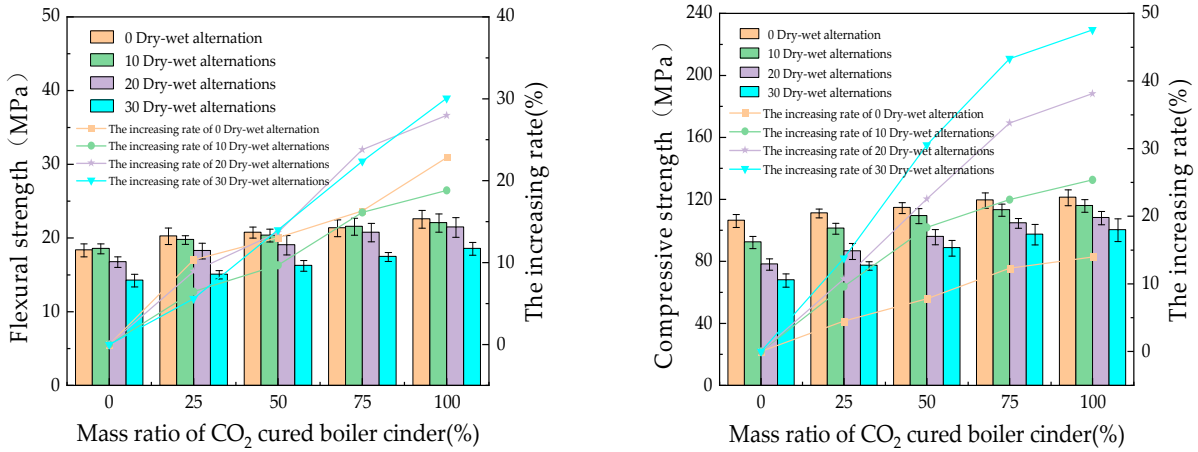

Figure 9. The mechanical strengths of RPC during NaCl D-A. (**a**) The flexural strength; (**b**) the compressive strength.

3.4. The SEM of RPC with CO_2-Cured Boiler Cinder

SEM photos of RPC with CO_2-cured boiler cinder (BC) are shown in Figure 10. As observed in Figure 10, the tightly packed hydration products are found in the microscopic images. As depicted in Figure 10, the flocculent hydration products decrease and the compact hydration products increase with increasing CO_2-cured boiler cinder. When CO_2-cured boiler cinder is added, the inner cracks in RPC are decreased. As discovered in Figure 10, the compactness of the hydration products are improved by the addition of CO_2-cured boiler cinder.

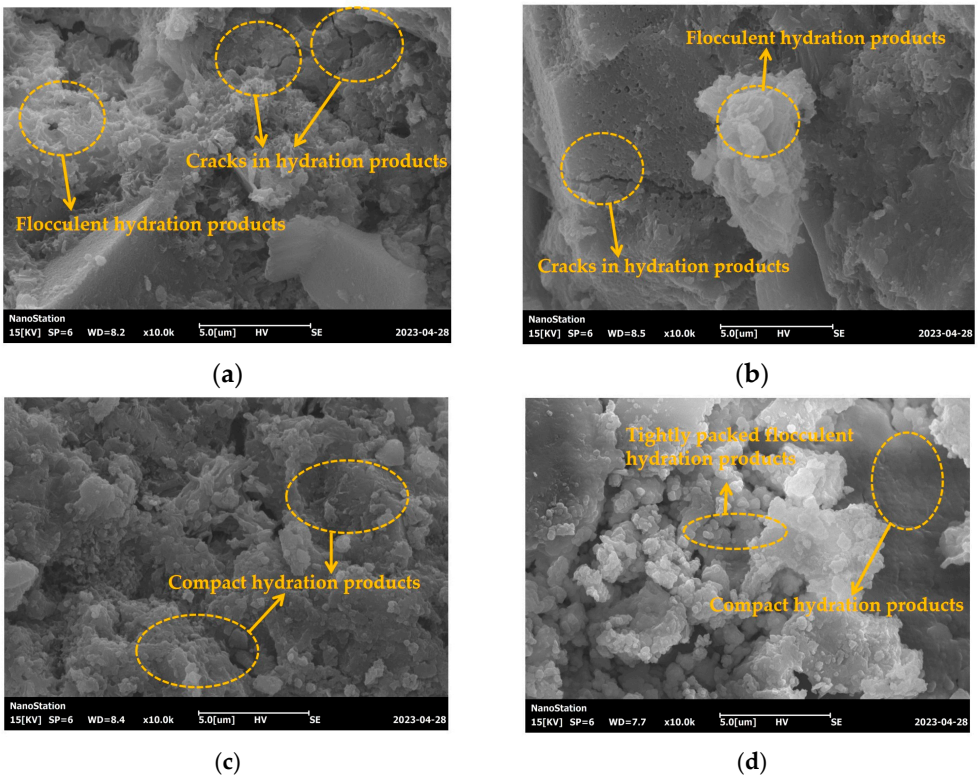

Figure 10. *Cont.*

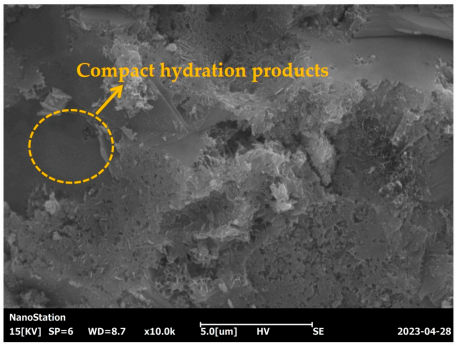

(**e**)

Figure 10. SEM photos of RPC with CO_2-cured BC. (**a**) RPC with 0% CO_2-cured BC, (**b**) RPC with 25% CO_2-cured BC, (**c**) RPC with 50% CO_2-cured BC, (**d**) RPC with 75% CO_2-cured BC, (**e**) RPC with 100% CO_2-cured BC.

3.5. The Thermal Analysis of RPC with CO_2-Cured Boiler Cinder

The TG curves of RPC with CO_2-cured boiler cinder are shown in Figure 11. As depicted in Figure 11, the TG decreases in the form of power function with the increasing temperature. The variation of TG curves can be divided into three steps. In the first step, the temperature varies from 31.2 to 150.2 °C. In this stage, the TG decreases due to the loss of free water during temperature rise. In the second step (temperature ranges from 150.2 to 474.1 °C), the value of the TG decreases with the increasing temperature. This is attributed to the disintegration of calcium hydroxide. During the third step, the temperature varies from 474.1 to 753.2 °C, and the TG decreases with the increasing temperature, which is ascribed to calcium carbonate. Additionally, the TG values are decreased by adding CO_2-cured boiler cinder, which is attributed to the fact that silicon oxide can play a nucleation role and participate in hydration, leading eventually to improving the hydration degree [33]. Moreover, the CO_2 curing on boiler cinder can result in reducing the corresponding particles' size and increasing the specific surface area, which can be capable of adsorbing cement ions and inducing nucleation and growth.

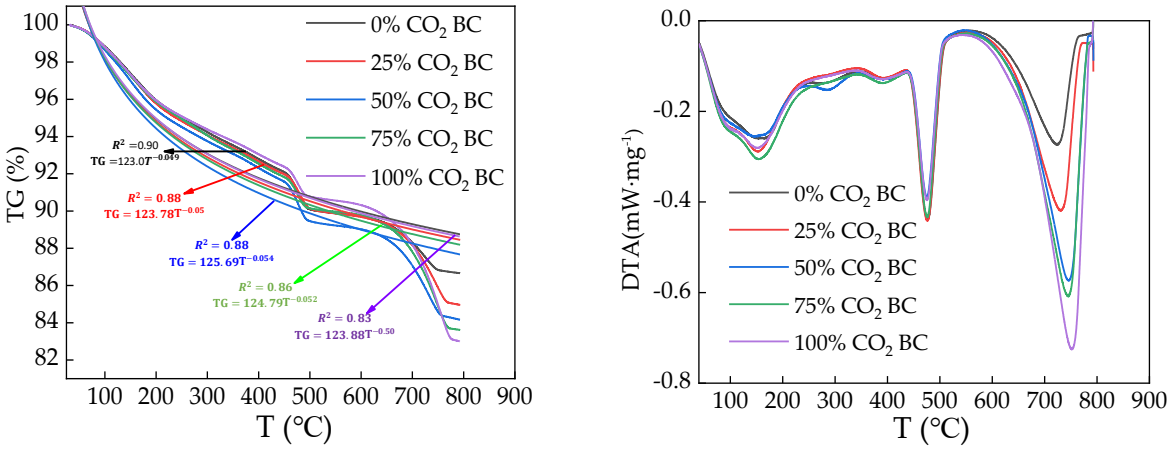

(**a**) (**b**)

Figure 11. The thermal analysis curve of RPC with CO_2-cured BC. (**a**) TG curves of RPC; (**b**) DTA curves of RPC.

3.6. The XRD Curves of RPC with CO_2-Cured Stove Ash

The XRD curves of RPC with CO_2-cured boiler cinder are shown in Figure 10. As found in Figure 12, the diffraction peaks of $3CaO{\cdot}SiO_2$(C_3S), $2CaO{\cdot}SiO_2$ (C_2S), cristobalite (SiO_2), and calcium hydroxide (CH) are observed in Figure 12. As exhibited in Figure 10, the diffraction peaks of C_3S and CH are decreased with the increasing curing age and the

addition of CO_2-cured boiler cinder. This can be ascribed to the fact that the addition of boiler cinder can promote the hydration of cement, thus decreasing the amount of C_3S. Moreover, the increasing amount of boiler cinder can increase the secondary hydration of cement. Furthermore, the CO_2 curing on boiler cinder can further decrease C_3S and CH due to the effect of CO_2-cured boiler cinder on the cement hydration.

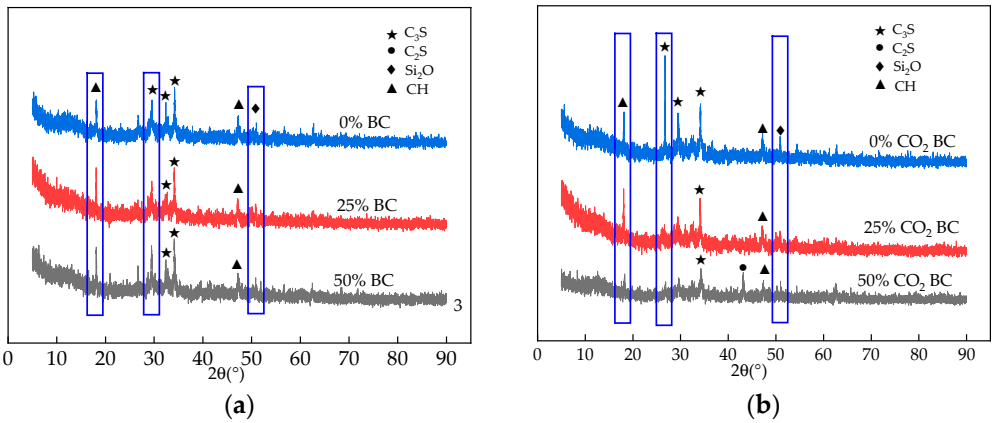

Figure 12. The XRD curves of RPC with CO_2-cured BC. (**a**) The XRD curves of RPC with BC; (**b**) the XRD curves of RPC with CO_2-cured BC.

4. Conclusions

This study aims to investigate the influence of CO_2-cured boiler cinder on the mechanical strength of RPC during NaCl action. This study can provide new ideas for handling boiler cinder and can also prove whether RPC with boiler cinder is suitable for marine concrete. The research conclusions can be summarized as follows.

During NaCl erosion, the relationship between the mass loss rate and the mass ratio of CO_2-cured boiler cinder fits the quadratic equation. Meanwhile, CO_2-cured boiler cinder can decrease the mass loss rate of RPC. After NaCl action, the mass loss rates are 0%–5.3%, and the mass loss rates' decreasing rate by CO_2-cured boiler cinder is 0%–51.3%. Meanwhile, the relationship between the RDEM and the mass ratio of CO_2-cured boiler cinder fits the quadratic equation, and CO_2-cured boiler cinder can increase the RDEM of RPC.

The addition of CO_2-cured stove ash can improve the flexural and compressive strengths with the corresponding increasing rates of RPC by 13.1%–36.3% and 11.2%–50.4% after encountering NaCl erosion.

The SEM, thermogravimetric analysis results, and XRD results confirm that the addition of CO_2-cured boiler cinder can improve the compactness of RPC and decrease the inner cracks. Moreover, as obtained from the thermogravimetric analysis results, CO_2-cured boiler cinder can decrease the values of the TG.

It can be obtained from the research results that CO_2-cured boiler cinder can be applied to manufacturing RPC. The CO_2 curing on boiler cinder can help improve RPC's resistance to NaCl erosion. Therefore, RPC with CO_2-cured boiler cinder suits the application of marine engineering.

Author Contributions: Methodology, L.B. and H.W.; Software, H.L.; Validation, L.B. and H.L.; Resources, L.B.; Writing—original draft, L.B.; Writing—review & editing, H.W.; Project administration, H.W. All authors have read and agreed to the published version of the manuscript.

Funding: The Zhejiang Provincial Natural Science Foundation [LY22E080005] and Ningbo Natural Science Foundation.

Institutional Review Board Statement: Not applicable.

Informed Consent Statement: Not applicable.

Data Availability Statement: Not applicable.

Conflicts of Interest: The authors declare no conflict of interest.

References

1. Liu, B.; Meng, H.; Pan, G.H.; Zhou, H. Relationship between the fineness and specific surface area of iron tailing powder and its effect on compressive strength and drying shrinkage of cement composites. *Constr. Build. Mater.* **2022**, *357*, 129421. [CrossRef]
2. Haselbach, L.; Valavala, S.; Montes, F. Permeability predictions for sand clogged Portland cement pervious concrete pavement systems. *J. Environ. Manag.* **2005**, *81*, 42–49. [CrossRef] [PubMed]
3. Han, F.H.; Luo, A.; Liu, J.H.; Zhang, Z.Q. Properties of high-volume iron tailing powder concrete under different curing conditions. *Constr. Build. Mater.* **2020**, *241*, 118108. [CrossRef]
4. Han, F.H.; Zhang, H.B.; Liu, J.H.; Song, S.M. Influence of iron tailing powder on properties of concrete with fly ash. *Powder Technol.* **2022**, *398*, 117132.
5. Zhang, Y.N.; Li, Z.J.; Gu, X.W.; Zhang, L. Utilization of iron ore tailings with high volume in green concrete. *J. Build. Eng.* **2023**, *72*, 106585. [CrossRef]
6. Liu, W.Z.; Niu, S.W. Energy evolution properties and strength failure criterion of coal-fired slag concrete based on energy dissipation. *Case Stud. Constr. Mater.* **2022**, *17*, e01369. [CrossRef]
7. Gu, X.W.; Zhang, W.F.; Zhang, X.L.; Qiu, J.P. Hydration characteristics investigation of iron tailings blended ultra high performance concrete: The effects of mechanical activation and iron tailings content. *J. Build.* **2022**, *45*, 103459. [CrossRef]
8. Supino, S.; Malandrino, O.; Testa, M.; Sica, D. The manufacturing of cement can cost large amount of energy and resources. *J. Clean. Prod.* **2016**, *112*, 430–442. [CrossRef]
9. Xu, F.; Wang, X.L.; Li, T.; Li, B.B.; Zhou, Y.; Liu, B. Mechanical properties and pore structure of recycled aggregate concrete made with iron ore tailings and polypropylene fibers. *J. Build.* **2021**, *33*, 101572. [CrossRef]
10. Wu, R.D.; Zhang, Y.Y.; Zhang, G.Y.; An, S.H. Enhancement effect and mechanism of iron tailings powder on concrete strength. *J. Build.* **2022**, *57*, 104954. [CrossRef]
11. Cui, L.; Wang, H. Influence of Waste Fly Ash on the Rheological Properties of Fresh Cement Paste and the Following Electrical Performances and Mechanical Strengths of Hardened Specimens. *Coatings* **2021**, *11*, 1558. [CrossRef]
12. Cui, L.; Wang, H. Research on the Mechanical Strengths and the Following Corrosion Resistance of Inner Steel Bars of RPC with Rice Husk Ash and Waste Fly Ash. *Coatings* **2021**, *11*, 1480. [CrossRef]
13. Du, Y.; Hao, W.; Shi, F.; Wang, H.; Xu, F.; Du, T. Investigations of the Mechanical Properties and Durability of Reactive Powder Concrete Containing Waste Fly Ash. *Buildings* **2022**, *12*, 560. [CrossRef]
14. Huang, F.; Qi, S.S.; Cheng, Y.H.; Li, W.C. Durability of concrete incorporated with siliceous iron tailings. *Constr. Build. Mater.* **2020**, *242*, 118147.
15. Lv, Y.; Yang, L.; Wang, J.; Zhan, B.; Xi, Z.; Qin, Y.; Liao, D. Performance of ultra-high-performance concrete incorporating municipal solid waste incineration fly ash. *Case. Stud. Constr. Mater.* **2022**, *17*, e01155. [CrossRef]
16. Feng, W.P.; Dong, Z.J.; Yu, J. Comparison on micromechanical properties of interfacial transition zone in concrete with iron ore tailings or crushed gravel as aggregate. *J. Clean. Prod.* **2021**, *319*, 12937. [CrossRef]
17. Liu, J.H.; An, S.H.; Zhang, Y.Y. Mechanism of regulating the mechanical properties and paste structure of supersulfated cement through ultrafine iron tailings powder. *Cem. Concr. Compos.* **2023**, *140*, 105061. [CrossRef]
18. Cheng, Y.H.; Sun, X.H.; Zhang, J.Y. Hydration kinetics of cement–iron tailing powder composite cementitious materials and pore structure of hardened paste. *Constr. Build. Mater.* **2023**, *370*, 130673.
19. Li, Y.; Li, X.; Tan, Y. Effect of aging on fatigue performance of cement emulsified asphalt repair material. *Constr. Build. Mater.* **2021**, *292*, 123417. [CrossRef]
20. Huang, S.B.; Pi, Z.J.; Cai, C.; Li, H. Utilization of high-sulfur iron ore tailings in cement mortar by considering the influence of curing temperature and tailing content. *J. Build. Eng.* **2023**, *74*, 106826. [CrossRef]
21. Zhao, B.; Wang, G.; Wu, B.; Kong, X. A study on mechanical properties and permeability of steam-cured mortar with iron-copper tailings. *Constr. Build. Mater.* **2023**, *383*, 131372. [CrossRef]
22. *GB/T 17671-1999*; Method of Testing Cements-Determination of Strength. The State Bureau of Quality and Technical Supervision: Beijing, China, 1999.
23. *GB/T50082-2009*; Standard for Test Method of Long-Term Performance and Durability of Ordinary Concrete. General Administration of Quality Supervision, Inspection and Quarantine of the People's Republic of China: Beijing, China, 2009.
24. Li, Z.; Zhang, W.; Jin, H.; Fan, X.; Liu, J.; Xing, F.; Tang, L. Research on the durability and Sustainability of an artificial lightweight aggregate concrete made from municipal solid waste incinerator bottom ash (MSWIBA). *Const. Build. Mater.* **2023**, *365*, 129993. [CrossRef]
25. Medina, C.; Rojas ML, S.; Frias, M. Freeze-thaw durability of recycled concrete containing ceramic aggregate. *J. Clean. Prod.* **2013**, *40*, 151–160. [CrossRef]
26. Li, L.J.; Liu, Q.F.; Tang, L.P.; Hu, Z.; Wen, Y.; Zhang, P. Chloride penetration in freeze–thaw induced cracking concrete: A numerical study. *Constr. Build. Mater.* **2021**, *302*, 124291. [CrossRef]
27. Xie, W.; Li, H.; Yang, M.; He, L.; Li, H. CO_2 capture and utilization with solid waste. *J. Clean. Prod.* **2022**, *3*, 199–209. [CrossRef]

28. Peys, A.; Snellings, R.; Peeraer, B.; Vayghan, A.G.; Sand, A.; Horckmans, L.; Quaghebeur, M. Transformation of mine tailings into cement-bound aggregates for use in concrete by granulation in a high intensity mixer. *J. Clean. Prod.* **2022**, *366*, 132989. [CrossRef]
29. Protasio, F.N.M.; Avillez, R.R.D.; Letichevsky, S.; Silva, F.D.A. The use of iron ore tailings obtained from the Germano dam in the production of a sustainable concrete. *J. Clean. Prod.* **2021**, *278*, 123929. [CrossRef]
30. Wang, H.; Shi, F.; Shen, J.; Zhang, A.; Zhang, L.; Huang, H.; Liu, J.; Jin, K.; Feng, L.; Tang, Z. Research on the self-sensing and mechanical properties of aligned stainless steel fifiber reinforced reactive powder concrete. *Cem. Concr. Compos.* **2021**, *119*, 104001. [CrossRef]
31. Ma, Z.M.; Liu MDuan, Z.H.; Liang, C.F.; Wu, H.X. Effects of active waste powder obtained from C&D waste on the microproperties and water permeability of concrete. *J. Clean. Prod.* **2020**, *257*, 120518.
32. Liska, M.; Jin, F.; Yi, Y.; Al-Tabbaa, A. Mechanism of reactive magnesia-ground granulated blastfurnace slag (GGBS) soil stabilization. *Can. Geotech. J.* **2016**, *53*, 773–782.
33. Wong, G.; Fan, X.; Gan, M.; Ji, Z.; Ye, H.; Zhou, Z.; Wang, Z. Resource utilization of municipal solid waste incineration fly ash in iron ore sintering process: A novel thermal treatment. *J. Clean. Prod.* **2020**, *263*, 121400. [CrossRef]